Polymer Chemistry

ROYAL SOCIETY OF CHEMISTRY

PAPER

View Article Online
View Journal

Cite this: DOI: 10.1039/d6py00073h

C_2-Symmetric H-bonding benzene core motif promotes rapid growth of long supramolecular fibers from amphiphilic polymers

Sebastian Städter, [a] Hesam Makki, [b] Ulrich Mansfeld, [c] Stephanie Hoeppener, [d,e] Albena Lederer [f,g] and Johannes C. Brendel *[a,c]

Strong hydrogen bonds are key non-covalent interactions that direct molecules into ordered supramolecular assemblies. C_3-symmetric benzene derivatives are a widely used motif to generate building blocks for helical supramolecular fibers, including amphiphilic supramolecular polymer bottlebrushes. In this work, we introduce the benzene diurea monoamide (BDUA) motif, which disrupts the C_3-core symmetry by combining distinct hydrogen bonding units. This design substantially simplifies the synthesis of amphiphilic building blocks, enabling multi-gram-scale preparation under mild conditions and avoiding labor-intensive purification procedures. The assembly behavior of BDUA amphiphiles was evaluated through quantum chemical calculations and extensive experimental screening. Computational analysis indicates that, despite the C_2-symmetric core substitution pattern, BDUA monomers form strong hydrogen bonds and adopt a helical organization within the supramolecular structure. When transferred into water, these amphiphiles rapidly assemble into long supramolecular fibers, even when initially dissolved in organic solvents and subsequently quenched into aqueous media. Compared to previously reported C_3-core symmetric benzene-based amphiphilic polymer building blocks, BDUA exhibits markedly accelerated assembly kinetics while preserving a non-dynamic, kinetically trapped fiber structure in water once assembled. Overall, the BDUA motif provides a synthetically scalable and highly effective platform for rapidly generating well-defined supramolecular polymer fibers, offering an easily accessible alternative to traditional C_3-core symmetric structures.

Received 23rd January 2026,
Accepted 13th May 2026

DOI: 10.1039/d6py00073h

rsc.li/polymers

Introduction

In nature, organisms exhibit a wide range of morphologies, which are often closely associated with their function.[1,2] Researchers started to investigate the structure–function relationships of nature's creations therby providing essential insights for the design of application-oriented materials. Although bioinspired materials can be fabricated in many dimensions, hierarchical one-dimensional structures are in particular of interest given their relevance to various fields ranging from biomedical science to chemical engineering.[3–6] In particular, supramolecular approaches have shown notable potential in forming anisotropic, elongated architectures *via* non-covalent forces.[7–11] Over the past decades, the underlying mechanisms of supramolecular polymerization have been thoroughly studied and provided fundamental knowledge and guidance.[12–16] Moreover, molecular design is widely acknowledged as a critical factor governing the self-assembly process and dictating the system properties and performance.[17,18] While preferably focusing on a certain type of non-covalent interactions, a broad range of molecule classes can be applied for the formation of one-dimensional supramolecular polymers.[12,19] Among benzene-derived molecular motifs, benzene trisamides (BTAs) represent a well-established system that has been examined in detail in numerous studies.[20–27] Upon directed hydrogen bonding of the three amide groups, BTAs form stacks inducing aggregation into larger cylindrical columns due to the preferred minimization of the surface and macrodipoles. Notably, the nature of intermolecular inter-

[a]Macromolecular Chemistry, University of Bayreuth, Universitätsstraße 30, 95447 Bayreuth, Germany. E-mail: johannes.brendel@uni-bayreuth.de
[b]Department of Chemical Engineering, University of Bath, Bath, BA2 7AY, UK
[c]Institute of Macromolecular Research (BIMF) and Bavarian Polymer Institute (BPI), University of Bayreuth, Universitätsstraße 30, 95447 Bayreuth, Germany
[d]Laboratory of Organic and Macromolecular Chemistry (IOMC), Friedrich Schiller University Jena, Humboldtstraße 10, 07743 Jena, Germany
[e]Jena Center for Soft Matter (JCSM), Friedrich Schiller University Jena, Philosophenweg 7, 07743 Jena, Germany
[f]Department Advanced Macromolecular Structure Analysis, Leibniz-Institut für Polymerforschung, Hohe Str. 6, 01069 Dresden, Germany
[g]Department of Chemistry and Polymer Science, Stellenbosch University, Private Bag X1, Matieland 7599, South Africa

actions plays a decisive role in shaping the three-dimensional arrangement of supramolecular assemblies. Already low-molecular-weight compounds are capable of forming lateral aggregates in accordance with the core-type assembly model.[28–31] The concept has likewise been proven adaptable to core–shell systems through the inclusion of hydrophilic groups, while preserving the original C_3-symmetrical design.[11,32–34] As a conceptual extension of this design, our group created amphiphilic supramolecular motifs, which combine C_3-symmetric cores with a hydrophilic polymer chain to create a typical amphiphile.[35] While the initial attempt based on BTA as core did not lead to cylindrical assemblies, the concept was refined and extended to benzene trisureas (BTUs) and benzene trispeptides (BTPs).[36,37] Through this approach, we achieved enhanced hydrogen bonding capabilities, resulting in more robust and extended fiber structures than those formed by BTAs. These systems exhibit remarkable flexibility in the orientation of both the core and peripheral chains, a property that we believe facilitates their aggregation into hierarchically organized fibers. In particular, the synergy between amphiphilic self-assembly in water and strong, directional hydrogen bonding within these building blocks appears crucial for the formation of stable, kinetically trapped fibers, whereas the incorporation of multiple sterically demanding hydrophilic polymers impedes the preferred hierarchical aggregation and, consequently, cylindrical assembly. While these studies clarified the impact of side-chain variations on self-assembly, the impact of symmetry within the hydrogen-bond forming core has yet been barely investigated. In particular, the presence of different hydrogen bonding groups within a single core motif introduces substantial complexity, leading to significant uncertainty in stack orientation under the given steric restrictions by the amphiphilic nature of the whole building block. Additionally, Li *et al.* introduced C_2-symmetrical benzene-1-urea-3,5-biscarboxamide (BUBA) as an interesting alternative to C_3-symmetric benzene motifs expanding the design scope of supramolecular building blocks.[38] In their study, they highlighted the conformational and system specific differences between C_2- and C_3-symmetrical molecules in apolar solvents providing knowledge for further property adjustment of mixed assemblies. Inspired by their work, we here investigate benzene diurea monoamides (BDUAs) as a novel, readily accessible motif for designing amphiphilic supramolecular building blocks with a C_2-symmetric core unit (Fig. 1).

BDUA represents a C_2-symmetric core and amphiphilic architecture conceptually derived from BTAs and BTUs.[35,36] But in contrast to our established BTU and BTP systems, BDUA enables a significantly more straightforward synthesis of amphiphilic building blocks bearing a single hydrophilic polymer chain. The synthetic route avoids tedious purification steps and readily allows for upscaling, thereby substantially enhancing the application potential of this system compared to previous architectures.

We synthesized a small library of BDUAs with varying PEO content to systematically probe its impact on packing parameters and morphology. Thereby, we focused on mono-PEGylated molecules, as previous studies have shown that multi-PEGylated analogues do not support fiber formation.[36] The PEO chain was directly linked to the amide function *via* a short linker, as this represents the most straightforward synthetic approach, although attachment through a urea group would also be of interest but is synthetically more challenging. Furthermore, we comprehensively analyzed the self-assembly of the supramolecular building blocks under varying conditions using dynamic light scattering (DLS), asymmetrical flow field-flow fractionation (AF4) and cryogenic transmission electron microscopy (cryo-TEM). In addition, their dilution stability was probed using fluorescence correlation spectroscopy (FCS). As a complementary study to our experimental approach, *ab initio* calculations were conducted, which enable

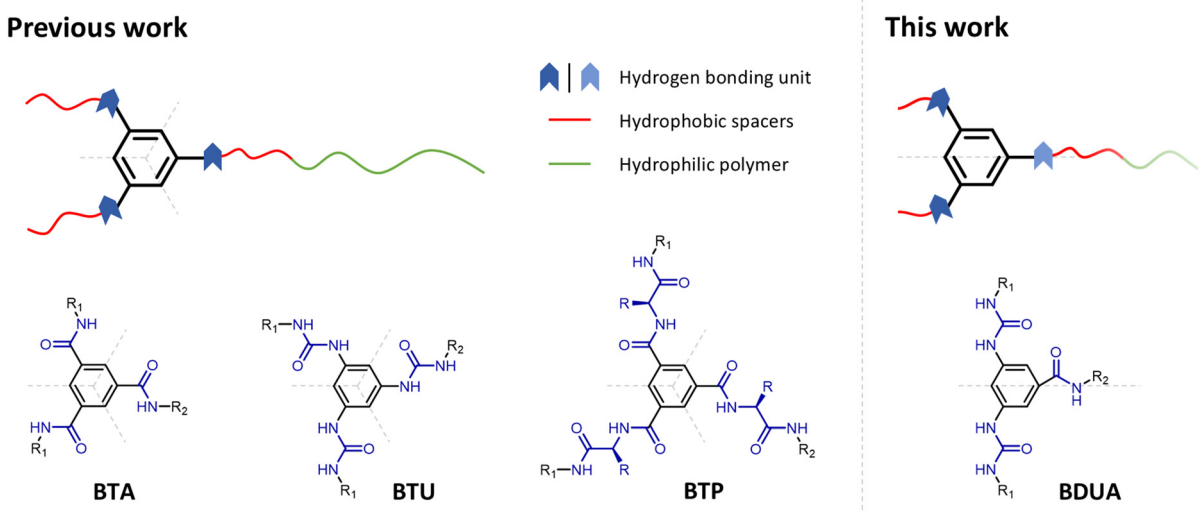

Fig. 1 Overview of benzene-based supramolecular motifs from earlier studies with identical hydrogen bonding units, highlighting structural features alongside a modified design for formation of BDUA with a C_2-symmetric core motif.[35–37,39,40]

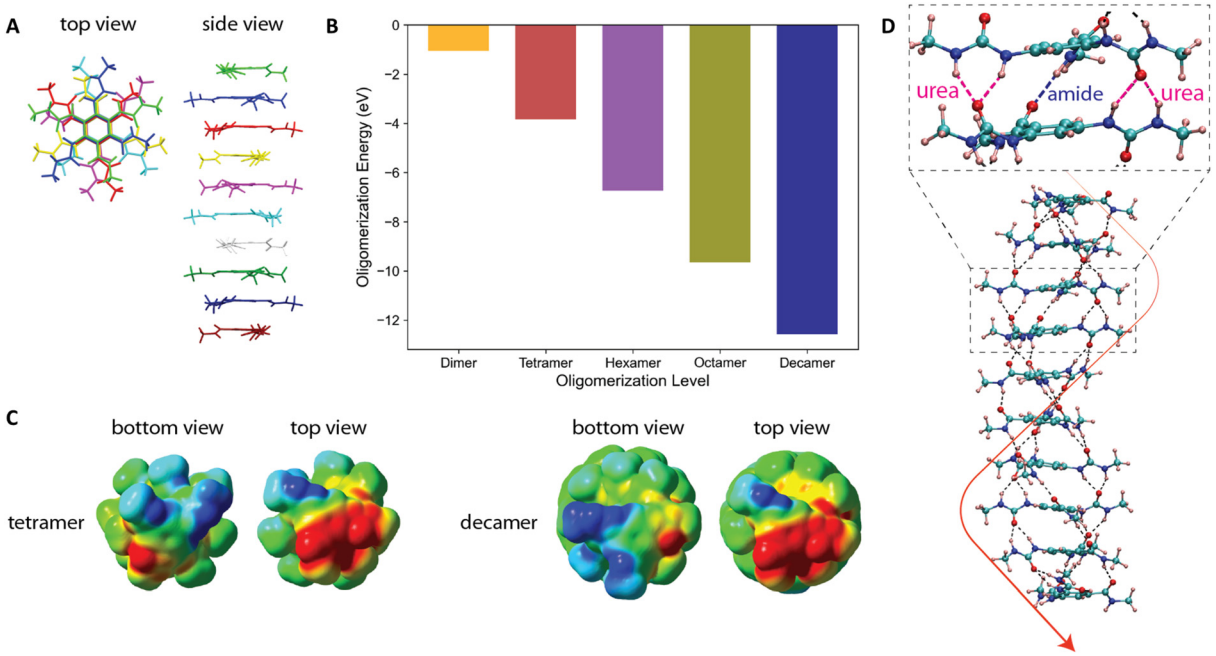

Fig. 2 (A): Top and side views of the initial configuration of a stack of 10 monomers with a 60° relative rotation angle. (B): Self-consistent field (SCF) energy of oligomerization, calculated as the SCF energy of the optimized oligomer minus the energy of the optimized monomer multiplied by the number of monomers in the oligomer. (C): Top and bottom views of the electrostatic potential map derived from the electron density around the tetramer and decamer, where red and blue regions represent positive and negative electrostatic potentials, respectively. (D): Helical orientation of the supramolecular assembly, with amide-amide and urea-urea hydrogen bonds indicated by dashed lines.

a comprehensive understanding of the intermolecular interactions of BDUAs.

Results and discussion

Density functional theory (DFT) calculations on the molecular assembly of benzene diurea monoamides

While C_3-symmetric BTAs are well studied for their stack formation, changing the symmetry can disrupt this process or lead to geometrically distinct aggregates, which might even impede fiber formation.[41,42] To clarify whether the altered hydrogen bonding topology of the BDUA motif still supports the formation of stable hydrogen-bonded stacks, we performed DFT calculations focusing on the intermolecular interactions within the hydrogen bonding core. In these calculations, the flexible peripheral substituents were omitted and the model was restricted to the comparatively rigid BDUA core. This simplification allows the analysis of the key directional hydrogen bonding interactions that govern stack formation while avoiding conformational contributions from long alkyl or polymer chains, which mainly affect higher-order aggregation rather than the local stacking motif.

First, the monomer geometry was optimized at the B3LYP/6-31G* level using Gaussian 16.[43,44] To explore possible self-assembly structures, we generated initial configurations of dimers to decamers with relative rotation angles ranging from −180° to 180° in 60° increments. An example of an initial configuration of a decamer with a 60° relative rotation angle is shown in Fig. 2A. DFT optimizations revealed that only the 60° relative rotation angle led to stable supramolecular structures, as indicated by the negative polymerization energy, suggesting a thermodynamically favorable process (Fig. 2B). Further insights from electron density analysis showed that polymerization induces a redistribution of electron density, enhancing electrostatic interactions and promoting cooperative growth, consistent with previous reports on different functionalized BTAs.[45] Fig. 2C presents top and bottom views of the tetramer and decamer, where red and blue regions indicate positive and negative electrostatic potential, respectively. A comparison between these structures reveals progressive polarization along the hydrogen-bonded chain: the top monomer in the tetramer exhibits a more negative electrostatic potential than in the decamer, while the bottom monomer in the decamer is more positively charged than in the tetramer. This observation suggests an overall polarization effect across the supramolecular assembly.

The most stable self-assembled structure (Fig. 2D) features a continuous hydrogen-bonded chain of monomers *via* interactions between amide and urea groups. In this context, the BDUA stack closely resembles another well-characterized C_2-symmetric core molecule, benzene-1-urea-3,5-biscarboxamide (BUBA).[38] However, the BDUA molecules show a mixed form of orientation for their hydrogen bonding units (preferentially oriented upwards/downwards with an 60° angle between monomers), which is rather unusual. Notably, no π–π stacking

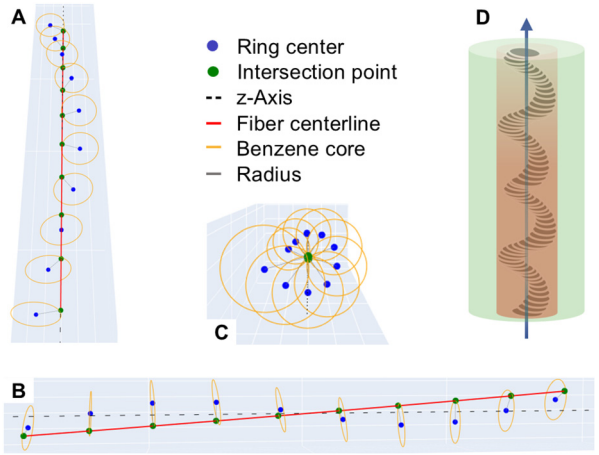

Fig. 3 Modeling of BDUA stacks in Python under the idealized assumption of circular benzene cores. Front view (A), side view (B), top view (C) and schematic representation (D).

was observed between the central benzene rings, likely due to the increased intermonomer distance and the central positioning of the molecules, which is dictated by hydrogen bonding. Furthermore, we observed average hydrogen bond distances of 1.88 Å and 1.95 Å between the amide and urea groups, suggesting a moderate electrostatic-covalent hydrogen bonding character, which is characteristic for this type of interaction.[25,46,47] The individual units adopt a tilted orientation relative to the stacking axis and assemble into a helical structure around it (Fig. 3). In a simplified macroscopic view, the stacked benzene cores define an inner hydrophobic cylinder.

Consequently, the computational results indicate that BDUA adopts a distinct spatial orientation and geometric conformation that arise solely from the selected hydrogen bonding topology, separating it from BTAs and BUBAs, while still maintaining assembly patterns akin to recognized supramolecular systems.

Synthesis and upscaling

Guided by the theoretical predictions, we further aimed to develop BDUA molecules mimicking the design principles of our BTU and BTP systems. Furthermore, a series of BDUAs bearing a hydrophilic PEO chain of 2, 5, or 10 kDa was prepared to assess the role of the theoretical packing parameter and steric constraints in shaping the assembly morphology. Earlier studies already confirmed, that these key features easily govern morphological transitions from cylindrical to spherical structures, prompting the question of whether BDUAs exhibit similar morphological behavior.[35,36,40] We derived a synthetic route (Scheme 1) to generate a C_2-symmetric core with two urea units and one amide starting from 3,5-diaminobenzoic acid, an inexpensive and commercially available compound.

Thereby, the precursor undergoes a reaction with dodecyl isocyanate in THF suspension, where precipitation of the insoluble intermediate **1** offers a simple and reliable visual cue for completion of reaction. The product was directly obtained through filtration at high purity. Yields were partially influenced by the isocyanate reactivity, but the filtrate purity was unaffected. The results remained consistent during scale-up, where a high yield of **85% (32.13 g)** could be achieved. The intermediate **2** is synthesized by applying efficient peptide coupling chemistry based on hexafluorophosphate benzotriazole tetramethyl uronium salt (HBTU) as coupling agent. The product was again obtained in high purity by filtration after precipitating the product in excess diethyl ether (DEE) achieving nearly a quantitative yield of **97% (46.30 g)**. In the following step, intermediate **3** was obtained using a standard Boc-deprotection protocol based on TFA. The reaction mixture was precipitated in excess DEE and the pure product was isolated by filtration/centrifugation. Overall, losses were minimized, resulting in a high yield of **95% (44.80 g)**. In the last step, PEGylation of the deprotected BDUA salt furnished the final products **4a–c**. Thereby, high purity is ensured due to the purification *via* membrane dialysis removing any unreacted traces of the starting material. Due to the high purity requirements

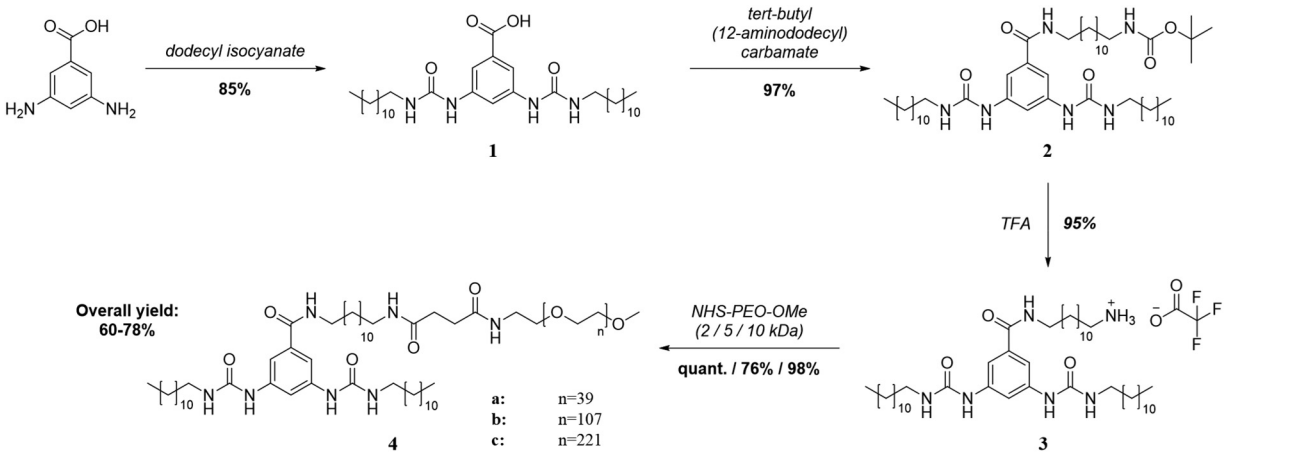

Scheme 1 Synthetic route for BDUAs. Detailed synthetic procedures can be found in SI.

for possible applications, the partially decreased yield associated with the dialysis process appears tolerable.

Overall, our synthetic strategy offers low manufacturing costs, facile purification, and highly favorable scale-up efficiency, providing overall yields in the range of 60 to 78%. Furthermore, this approach relies on established isocyanate and amide coupling chemistry, providing high modularity through the broad availability of commercially accessible building blocks. Compared to BTU and BTP systems, the multi-step preparation of BDUAs requires substantially less synthetic effort and can be readily automated. In addition, production on the kilogram scale or beyond appears feasible, provided that sufficient synthetic capacity is available.

Self-assembly in an aqueous environment

As noted above, the BDUA building blocks were designed analogously to our previously reported amphiphilic systems based on C_3-symmetric cores (BTU and BTP). To enable a direct comparison of structure formation, we applied the same self-assembly conditions established in these earlier studies.[40] Accordingly, the products **4a–4c** were either directly dispersed (dd) in water or their self-assembly was induced through a solvent switch (sw) procedure. In the latter case, the compounds were first dissolved in tetrahydrofuran (THF), which as a good solvent prevents high-order stacking.[48] Then, water was added at specific rates enhancing the intermolecular interactions of the BDUA molecules due to the hydrophobic effect.[49] Thereby, the surface of the hydrophobic parts are minimized, resulting in a core–shell assembly, where the outer hydrophilic surface shields the inner core (Fig. 4).

As a result of only small variations in the molecule design, we observed similarities in the aggregation behavior of BDUAs compared to our previously published BTUs and BTPs, meaning that the onset for the nucleation-elongation process is triggered by crossing a certain critical water content.[40] In case of BDUA, a critical water content is reached between 50 to 60 v% of D_2O, as indicated by ^{1}H-NMR studies across different ratios of d_8-THF : D_2O (Fig. S4). It is interesting to note that this transition is rather sharp compared to previous results on BTPs.[50] Up to 50 v%, the ^{1}H signals for the benzene core appear unchanged indicating a good solubility or at least rapid kinetic exchange. However, crossing to 60 v% of D_2O results in an immediate disappearance of the aromatic signals as a result of the full aggregation of the building blocks. The supramolecular polymerization begins once this threshold is exceeded, progressing rapidly until a thermodynamically favorable state is reached. Despite being described as an immediate process, the narrow area around the critical water content is important for the control of the morphology.[51,52] As a result, approaching the critical water content with varying but defined rates is of high interest and was further investigated by performing solvent switches with modified water addition rates. Therefore, we prepared individual dispersions of **4a–c** at 1/50/100 mL h^{-1} as well as direct dispersions (dd) of the powdered material in water, which were first analyzed with dynamic light scattering (Fig. S5 and Table S2). In general, a broad distribution in size can be observed for all rates indicating differences in diffusive behavior and/or multiple species. For **4a** different solution concentrations were prepared to investigate the influence on the assembly process. However, at first sight the summarized results show no observable trend, which is also attributed to the general limitations of DLS for the measurement of large, non-spherical particles.[53,54] Nevertheless, the size distribution curves are indicating that controlled solvent switches are providing better size control. Furthermore, minimal shifts of the peaks can be observed, suggesting a direct correlation between addition rate and size. In addition, the correlograms further prove the presence of larger aggregates, recognizable due to right shift and the downshift of the plateau. Here, also differences between direct dispersion and controlled addition are visible, suggesting a tendency towards larger aggregates under controlled conditions for **4a**.

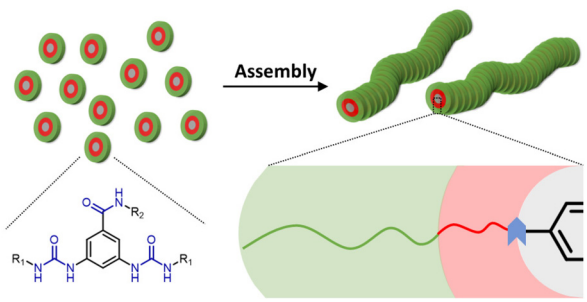

Fig. 4 Schematic illustration of BDUA assembly induced by solvent exchange from THF to water through hydrophobic shielding.

To overcome the limited information content of DLS data and for precise size, shape and morphology determination, selected samples were analyzed *via* AF4 (Fig. 5A–C and Fig. S6). Here, clear differences between direct dispersion and controlled conditions for compound **4a** are observed (Fig. S6A–D). In case of direct dispersion, the molecules are directly dissolved in a poor solvent. Therefore, nucleation and supramolecular polymerization are competing, leading to uncontrolled assembly behavior and mixed morphologies (Fig. S6A). In addition, dry-state structures that remain after the final purification can influence how the compound disperses, which may in turn affect the structure formation. While direct dispersion shows an R_g of approximately 52 nm, samples prepared under controlled solvent switch conditions yield R_g values of 130 to 150 nm and unimodal distributions (Table S3 and Fig. S6A–D). These results indicate that, in contrast to direct dispersion, solvent switch samples exhibit size uniformity that is independent of the addition rate. Moreover, shape factors (R_g/R_h) differing from 0.778 are suggesting the presence of an anisotropic morphology (Table S3).[55] However, the observed ratios are below 0.4, characteristic of microgels, and significantly smaller than the values (exceeding 2.2) associated with rod-like structures.[56] This observation can be explained by the broad DLS distribution, which elevates R_h, and may additionally reflect dense or aggregated structures under flow con-

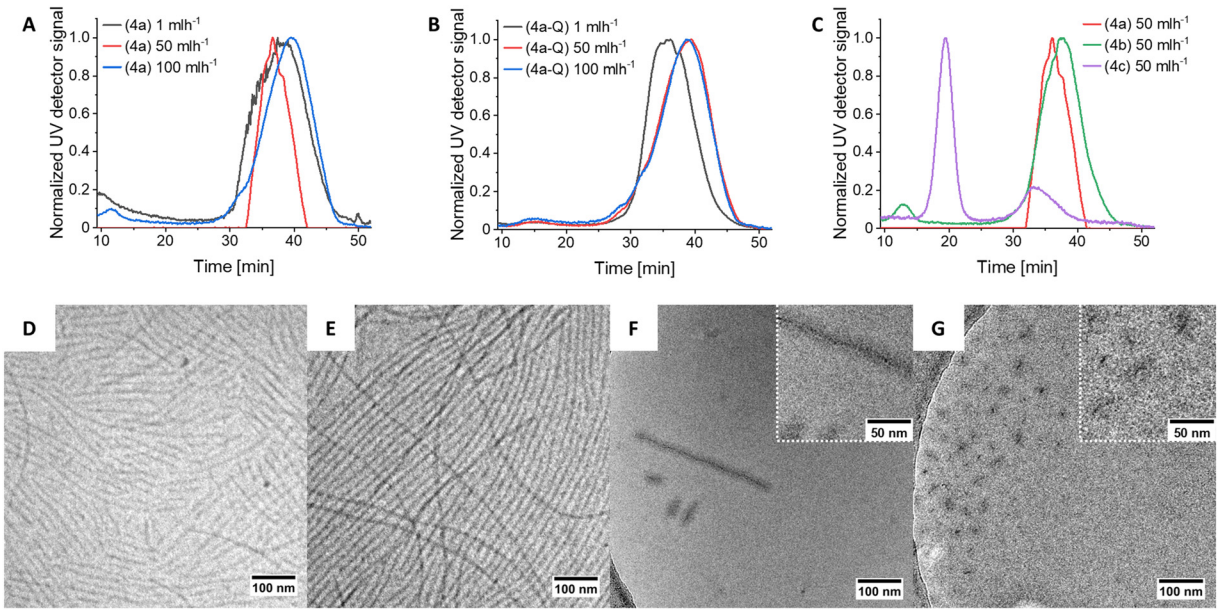

Fig. 5 AF4 fractograms (A–C) and cryo-TEM images (D–G) of selected samples. AF4 samples of compounds **4a–c** were prepared by solvent switch method (A and C) and quenching method (B). Cryo-TEM images were taken of selected samples prepared by direct dispersion or solvent switch method: **4a** dd (D), **4a** sw at 50 mL h^{-1} (E), **4b** sw at 50 mL h^{-1} (F) and **4c** sw at 50 mL h^{-1} (G).

ditions in AF4, which leads to a decrease in R_g. Nevertheless, the average lengths of **4a** assemblies with narrow distributions (Table S3), calculated from the derived R_g, agree well with the cryo-TEM observations, which were performed on selected samples to further elucidate morphology and to provide additional in-depth structural information (Fig. 5D and E).

Consistent with the AF4 results, shorter fibers are formed by applying direct dispersion. This could be attributed to the reintroduction of dry-state structures upon dispersion and potential fragmentation. In contrast, slow addition of water to a molecular solution of the building blocks allows a more controlled approaching of the critical water content (CWC) and therefore fiber elongation may be enhanced, and longer cylindrical aggregates can be assembled. Notably, both short and long fibers have a similar diameter of approximately 10.5 nm (Fig. S7C and D). Accordingly, BDUA exhibits an enlarged diameter compared to the related BTUs (7.3 nm ± 1.1 nm), despite having an otherwise identical design, differing only by the urea-to-amide substitution.[36]

A more general comparison regarding the self-assembly of BDUA building blocks with the previously reported BTUs and BTPs reveals some similarities but also major differences in the resulting structures. Considering that the supramolecular bottlebrushes made from BDUA exhibit a comparable diameter as BTU and BTP derived ones, their hydrophobic core cross-sections are likely composed of several laterally aggregated units surrounded by an outer PEO shell.[36,37] However, compared to the previously reported BTUs and BTPs, as well as other bisurea motifs, the assembly of BDUA **4a** results overall in remarkably long fibers which exceed the previous systems in length by far given equal assembly conditions.[37,40,57,58] Under direct dispersion conditions, BDUA fibers exhibit length scales of approximately 300 nm, comparable to BTUs, whereas BTPs remain shorter.[36,37] Through the solvent switch approach, BDUA forms fibers on the micrometer scale even at high addition rates, demonstrating that variations in the addition rate have only a minor impact on the BDUA system, in contrast to the behavior observed for BTU and BTP systems.[40] These results indicate very fast kinetics of the BDUA fiber growth once the CWC is reached.

In order to further investigate this aspect, we additionally investigated a quenching method where a THF-solution of the building block is dropped into water at different rates. In case of BTUs or BTPs, a similar quenching approach creates trapped morphologies and the formation of small, in many cases nearly spherical shaped aggregates.[40] In contrast to these systems, the quenching of BDUA **4a** results in unimodal distributions consistent with those obtained *via* the solvent switch method (Fig. 5B). Zimm-plot analysis of the scattering data revealed R_g values comparable to those of the solvent switch samples (Table S3 and Fig. S6E–G). Considering these stark differences in the assembly behavior compared to BTU or BTP and the obtained similar sizes of the aggregates, we consider that alternative assembly mechanisms may play a significant role in case of BDUA. While in the solvent switch still results in a nucleation and growth mechanism at a given CWC, also a critical THF content (CTC) might be crossed in the quenching approach, which induces a more dynamic state of the assemblies (Fig. 6). In this case, BDUA molecules might still form trapped small aggregates until the CTC is reached, but then the system becomes more dynamic and besides growth by further added building blocks existing small aggregates start

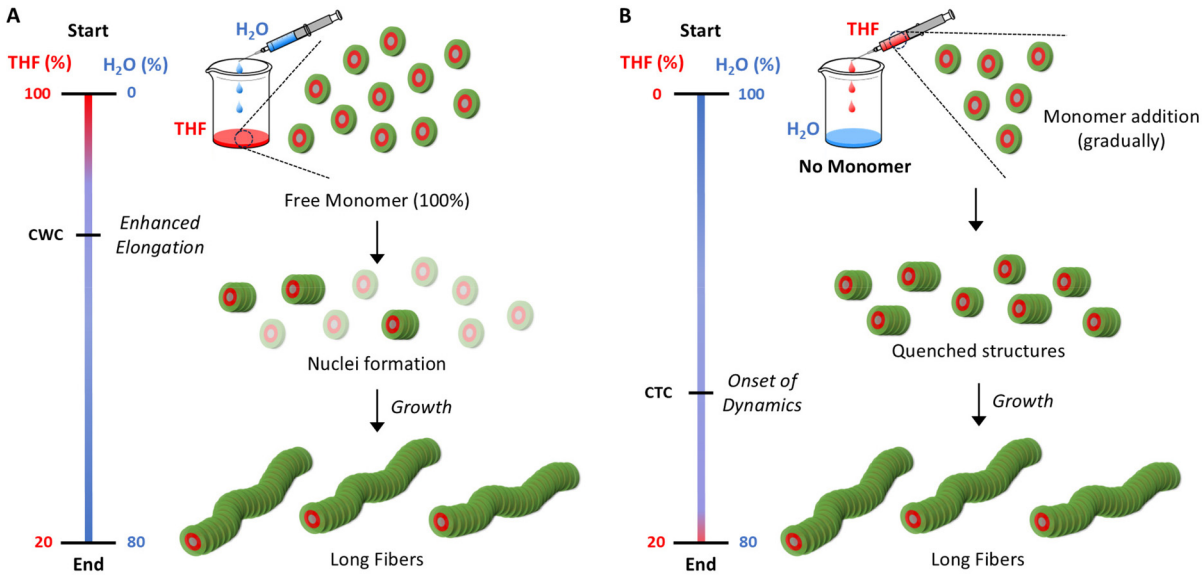

Fig. 6 Visualization of solvent switch (A) and quenching processes (B), providing insight into possible principles governing both. CWC: critical water content; CTC: critical THF content.

fusing or get dissolved in favor of further growth of larger structures. Unfortunately, a more detailed examination of the process requires *in situ* monitoring methods for such small aggregates, such as time-resolved neutron scattering, which is beyond our current capabilities. Nevertheless, owing to the subtle difference in hydrogen bonding topology while otherwise preserving the molecular design, BDUAs exhibit an extended performance scope compared with BTUs and BTPs. The results indicate rapid elongation, enabling the formation of long fibers even under quenching conditions. Overall, both assembly methods permit the precise formation of supramolecular fibers if controlled conditions are applied.

Variations in molecular design on the contrary lead to more significant differences in the resulting structures (Fig. 5C and Fig. S5D, E, S6I, J). In DLS, a decrease in size and distribution can be observed for **4b** and **4c** with an increasing length of the attached PEO. While the peaks of the size distribution curves show good separation here, clear shifts to the left of the correlograms can be observed in most cases indicating the presence of different morphologies, different ratios of existing morphologies and/or smaller aggregates compared to **4a**. In AF4, a trend towards a predominance of smaller species is observed when the length of the PEO chain is increased from **4a** to **4c**. Still, all fractions continue to exhibit larger aggregates within the same size range, and combined analysis of the light scattering data yields a shape factor greater than 2 for **4b** and **4c** indicating not only anisotropic structures but also the presence of rod-like assemblies (Table S3). The morphology was confirmed by cryo-TEM images (Fig. 5E–G), which also provided further structure-related insights. While Fig. 5E displays very dense and long fibers, a shortening of the cylindrical aggregates can be observed with an increasing PEO chain length in **4b** and even more pronounced in **4c**. The decrease of the overall fiber density in **4b** and **4c** compared to **4a** might be related to a decreased concentration of aggregates and may indicate the presence of non-aggregated building blocks, but effects of the preparation of the cryo-TEM samples cannot be fully excluded. Interestingly, the enhanced contrast in Fig. 5F and G allows the core and shell to be distinguished. The core diameter of **4b** and **4c** is similar, considering the resolution limit. Consequently, **4b** and **4c** still reveal fiber formation, although their lengths are considerably smaller appearing overall oval or round shaped. Therefore, the characteristic dependence of morphology on the packing parameter, previously observed for the BTU and BTP systems, is also retained for BDUA motifs, demonstrating that longer PEO chains suppress fiber formation.[36,37]

With regard to the previously mentioned dynamics during the assembly of the fibers, we were further interested in the stability of the BDUA assemblies, which could potentially restrict their application potential. In particular, highly diluted samples might reveal a molecular dissolution of the building blocks at very low concentrations which would only be possible if the assembly is in a dynamic equilibrium with the molecular dissolved state. Therefore, BDUA was labeled with AF488 and subjected to a serial dilution from micromolar to nanomolar concentrations, followed by analysis using fluorescence correlation spectroscopy (FCS). The method allows determination of diffusion coefficients at very low concentrations based on temporal fluctuations of fluorescence intensity in a confocal volume. The resulting autocorrelation function can be fitted to calculate a diffusion coefficient of the fluorescence species allowing differentiation between free labelled polymer chains and aggregated states. Autocorrelation data were collected for BDUA concentrations ranging from 1.03 μmol L^{-1} to 0.01 μmol L^{-1} in water, as well as for concentrations of 1.03 μmol L^{-1} in

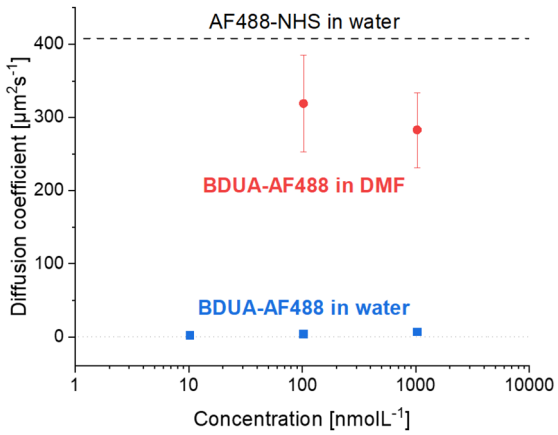

Fig. 7 Comparison of diffusion coefficients derived from autocorrelation data for the reference dye and the supramolecular motif in DMF and water. AF488-NHS was measured at 1.03 nmol L^{-1} and extrapolated for visualization purposes.

DMF (Fig. S8). For reference, autocorrelation data for AF488 in water was also measured. While the results for the aqueous BDUA solution were fitted with a conformational model, a pure diffusion model was occasionally applied for BDUA in DMF. The summarized data is shown in Table S4. From this analysis, a diffusion time of a few milliseconds for the aqueous BDUA solution is observed. In contrast, BDUA in DMF presents a diffusion time of 0.053 ± 0.001 ms, which is much closer to the reference solution of AF488 in water (0.030 ± 0.001 ms). Furthermore, the diffusion coefficients of all samples were calculated directly from the autocorrelation data (Fig. 7).

As a result, BDUA in DMF displays a high diffusion coefficient with an average value of 301 $\mu m^2\ s^{-1}$, indicating the presence of freely diffusing unimers. In contrast, the aqueous BDUA samples result in low diffusion coefficient below 10 $\mu m^2\ s^{-1}$ which confirms stable assemblies at these low concentrations and, therefore, indicates a non-dynamic character of the assembly in pure water. Based on the diffusion coefficients for BDUA-AF488 in water, fiber lengths were calculated (Table S5) using the extended Stokes–Einstein equation, following the Tirado and García de la Torre model.[59] The lengths determined by FCS exhibit a similar range to those obtained through AF4, with values typically ranging between 100 to 1000 nm. However, a more detailed comparison of the two methods regarding length determination is not pursued, as the FCS data exhibit significantly higher error potential and relate to a modified BDUA structure.

Conclusion

In summary, our results demonstrate that the C_2-symmetric core motif in BDUA not only facilitates self-assembly of corresponding amphiphilic building blocks into supramolecular bottlebrushes, but also significantly enhances aggregation kinetics resulting in the formation of long hierarchically structured fibers when compared to previously reported C_3-symmetric cores. Based on the theoretical predictions, the supramolecular polymerization of the BDUA is highly thermodynamically favored compared to the formation of low-numbered stacks due to the redistribution of electron density in addition to the known effects of hydrophobic shielding. Thereby, the molecules possess a rotational offset of 60°, forming moderate hydrogen bonds (1.88–1.95 Å) between amide and urea groups. Similar values and strong aggregation have been reported before for other members in the family of benzene based motifs, but also clear differences can be observed.[25,36,37,40,45] Although the steric hinderance is negligibly different compared to amide-, urea- and peptide analogues, the structural and DFT optimizations show different orientations (upwards/downwards) for the hydrogen bonding units. Furthermore, the individual units adopt a helical arrangement, with a tilted orientation relative to the stacking axis.

The analysis of assemblies in aqueous environments provided further insights into their individual behavior and characteristics. In particular, the DLS, AF4 and cryo-TEM data prove the successful formation of supramolecular bottlebrushes under various conditions. While direct dispersion leads to a mixture of morphologies including shorter fibers, the solvent switch approach from THF to water induces the formation of very long fibers if a PEO chain of 2 kDa is attached. Longer PEO chains result in steric hindrance and significant shortening of the aggregates similar as previously observed for corresponding C_3-core symmetric motifs (BTU and BTP). Interestingly, an analysis of the assembled hydrophobic cores in case of BDUA reveals a thickness independence of the assembly conditions or the PEO length indicating a similar core structure, in correspondence with other known peptide and bisurea systems.[36,37,40,57,58] This further indicates, that the hydrophobic core consists of multiple independent fibers with an outer PEO shell like known BTU stacks.[36] Besides these similarities, solvent switches at high water addition rate and more extreme quenching experiments also revealed stark differences of BDUA compared to other systems. The here presented C_2-symmetric core facilitates exclusively fiber formation even at quenching conditions resulting overall in very similar length of the fibers independent of the process conditions. This fact can either be related to a very rapid elongation process or may be a result of a dynamic exchange process and continuous growth by fiber fusing or molecular diffusion. While an *in situ* assembly study of such a rapid process was beyond this study, FCS analysis of labelled highly diluted samples reveals constantly low diffusion coefficients in order of magnitude expected for larger aggregates. These results therefore confirm a non-dynamic character of the aggregates in water and suggest that either the assembly process is extremely rapid or a critical THF content must be reached to induce dynamics. Further extended studies to elucidate the dynamics of these assemblies are in preparation, but in conclusion, this study clearly demonstrates that despite the break in the C_3-core symmetry of the hydrogen bonding core structure, strong

intermolecular interactions and sufficient driving forces can be induced with the BDUA motif to generate large supramolecular fibers with several micrometer length in water and high stability. In addition, the molecule is readily accessible in very few scalable synthetic steps with excellent yields circumventing any tedious purification steps, which gives it the potential to become a workhorse in the design of further application-oriented materials.

Conflicts of interest

There are no conflicts to declare.

Data availability

The data supporting this article are presented in the main manuscript or have been included as part of the supplementary information (SI). Synthetic procedures, associated measurements, and complementary analytical data including NMR, DLS, AF4, cryo-TEM, and FCS are provided in the SI. Supplementary information is available. See DOI: https://doi.org/10.1039/d6py00073h.

Acknowledgements

We thank the German Science Foundation (DFG) for generous funding within the Emmy-Noether Programme (Project-ID: 358263073) and the Heisenberg-Programme (Project-ID: 517761335). We further appreciate the support by the DFG within the collaborative research center SFB1278 "PolyTarget" (Project-ID: 316213987 – SFB 1278, Z01). TEM investigations were performed at the Keylab Electron and Optical Microscopy within the Bavarian Polymer Institute in Bayreuth and at the Electron Microscopy facilities of the Jena Center for Soft Matter (JCSM), which was established with grants from the DFG and the European Fund for Regional Development (EFRE). FCS measurements were carried out at the KeyLab Optical Spectroscopy within the Bavarian Polymer Institute in Bayreuth. We further acknowledge Sandra Opel and Agate Levron for their support synthesizing the building blocks and Dr Ceren Cokca Pihlamägi for proof reading. We also thank Alina Kasberg for performing the AF4 measurements, Dr Lisa Günther for carrying out the FCS measurements and Qi Yu for supplementary Python-based data analysis. Prof. U. S. Schubert is furthermore acknowledged for his support and access to research facilities at the FSU Jena.

References

1 M. A. R. Koehl, *Annu. Rev. Ecol. Evol. Syst.*, 1996, **27**, 501–542.
2 D. T. Kysela, A. M. Randich, P. D. Caccamo, *et al.*, *PLoS Biol.*, 2016, **14**(10), e1002565.
3 N. Zhao, Z. Wang, C. Cai, *et al.*, *Adv. Mater.*, 2014, **26**(41), 6994–7017.
4 Z. Li, M. Tang, S. Liang, *et al.*, *Prog. Polym. Sci.*, 2021, **116**, 101387.
5 X. Dou, N. Mehwish, C. Zhao, *et al.*, *Acc. Chem. Res.*, 2020, **53**(4), 852–862.
6 Y. Wang, J. Chou, Y. Sun, *et al.*, *Mater. Sci. Eng., C*, 2019, **101**, 650–659.
7 E. Gardey, Z. Cseresnyes, F. H. Sobotta, *et al.*, *Small*, 2024, **20**(21), 2306482.
8 D. Schröder, K. Kreger, U. Mansfeld, *et al.*, *Adv. Mater. Interfaces*, 2024, **11**(25), 2400259.
9 M. Weber, F. Bretschneider, K. Kreger, *et al.*, *Adv. Mater. Interfaces*, 2024, **11**(29), 2400101.
10 F. V. Gruschwitz, F. Hausig, P. Schüler, *et al.*, *Chem. Mater.*, 2022, **34**(5), 2206–2217.
11 S. Varela-Aramburu, G. Morgese, L. Su, *et al.*, *Biomacromolecules*, 2020, **21**(10), 4105–4115.
12 M. Hartlieb, E. D. H. Mansfield and S. Perrier, *Polym. Chem.*, 2020, **11**(6), 1083–1110.
13 A. Ciferri, *Macromol. Rapid Commun.*, 2002, **23**(9), 511–529.
14 T. F. A. De Greef, M. M. J. Smulders, M. Wolffs, *et al.*, *Chem. Rev.*, 2009, **109**(11), 5687–5754.
15 A. Sorrenti, J. Leira-Iglesias, A. J. Markvoort, *et al.*, *Chem. Soc. Rev.*, 2017, **46**(18), 5476–5490.
16 M. Wehner and F. Würthner, *Nat. Rev. Chem.*, 2020, **4**(1), 38–53.
17 J.-M. Lehn, *Angew. Chem., Int. Ed. Engl.*, 1988, **27**(1), 89–112.
18 J. M. Lehn, *Pure Appl. Chem.*, 1978, **50**(9–10), 871–892.
19 F. V. Gruschwitz, T. Klein, S. Catrouillet, *et al.*, *Chem. Commun.*, 2020, **56**(38), 5079–5110.
20 J. J. van Gorp, J. A. J. M. Vekemans and E. W. Meijer, *J. Am. Chem. Soc.*, 2002, **124**(49), 14759–14769.
21 P. J. M. Stals, M. M. J. Smulders, R. Martín-Rapún, *et al.*, *Chem. – Eur. J.*, 2009, **15**(9), 2071–2080.
22 P. J. M. Stals, J. C. Everts, R. de Bruijn, *et al.*, *Chem. – Eur. J.*, 2010, **16**(3), 810–821.
23 A. Bernet, R. Q. Albuquerque, M. Behr, *et al.*, *Soft Matter*, 2012, **8**(1), 66–69.
24 S. Cantekin, T. F. A. de Greef and A. R. A. Palmans, *Chem. Soc. Rev.*, 2012, **41**(18), 6125–6137.
25 C. Kulkarni, E. W. Meijer and A. R. A. Palmans, *Acc. Chem. Res.*, 2017, **50**(8), 1928–1936.
26 B. Wu, L. Liu, L. Zhou, *et al.*, *J. Colloid Interface Sci.*, 2022, **608**, 1297–1307.
27 Y. Zhang, H. Wang, Q. Li, *et al.*, *Soft Matter*, 2022, **18**(16), 3241–3248.
28 A. Frank, A. Bernet, K. Kreger, *et al.*, *Soft Matter*, 2020, **16**(19), 4564–4568.
29 Y. Nakano, T. Hirose, P. J. M. Stals, *et al.*, *Chem. Sci.*, 2012, **3**(1), 148–155.
30 P. J. M. Stals, J. F. Haveman, A. R. A. Palmans, *et al.*, *J. Chem. Educ.*, 2009, **86**(2), 230.
31 C. F. C. Fitié, W. S. C. Roelofs, P. C. M. M. Magusin, *et al.*, *J. Phys. Chem. B*, 2012, **116**(13), 3928–3937.

32 R. P. M. Lafleur, S. Herziger, S. M. C. Schoenmakers, *et al.*, *J. Am. Chem. Soc.*, 2020, **142**(41), 17644–17652.
33 B. N. S. Thota, X. Lou, D. Bochicchio, *et al.*, *Angew. Chem., Int. Ed.*, 2018, **57**(23), 6843–6847.
34 C. M. A. Leenders, L. Albertazzi, T. Mes, *et al.*, *Chem. Commun.*, 2013, **49**(19), 1963–1965.
35 T. Klein, F. V. Gruschwitz, S. Rogers, *et al.*, *J. Colloid Interface Sci.*, 2019, **557**, 488–497.
36 F. V. Gruschwitz, M.-C. Fu, T. Klein, *et al.*, *Macromolecules*, 2020, **53**(17), 7552–7560.
37 T. Klein, H. F. Ulrich, F. V. Gruschwitz, *et al.*, *Polym. Chem.*, 2020, **11**(42), 6763–6771.
38 Y. Li, L. Dubreucq, B. G. Alvarenga, *et al.*, *Chem. – Eur. J.*, 2019, **25**(45), 10650–10661.
39 H. F. Ulrich, F. V. Gruschwitz, T. Klein, *et al.*, *Chem. – Eur. J.*, 2024, **30**(26), e202400160.
40 F. V. Gruschwitz, T. Klein, M. T. Kuchenbrod, *et al.*, *ACS Macro Lett.*, 2021, **10**(7), 837–843.
41 L. Bouteiller, O. Colombani, F. Lortie, *et al.*, *J. Am. Chem. Soc.*, 2005, **127**(24), 8893–8898.
42 J. J. Van Gorp, J. A. J. M. Vekemans and E. W. Meijer, *Mol. Cryst. Liq. Cryst.*, 2003, **397**(1), 191–205.
43 M. J. Frisch, G. W. Trucks and H. B. Schlegel, *et al.*, *Gaussian 16, Revision C.01*, Gaussian, Inc., Wallingford CT, 2016.
44 P. C. Hariharan and J. A. Pople, *Theor. Chim. Acta*, 1973, **28**(3), 213–222.
45 I. A. W. Filot, A. R. A. Palmans, P. A. J. Hilbers, *et al.*, *J. Phys. Chem. B*, 2010, **114**(43), 13667–13674.
46 G. A. Jeffrey, *An Introduction to Hydrogen Bonding*, Oxford University Press, 1997.
47 G. Gilli and P. Gilli, *The Nature of the Hydrogen Bond: Outline of a Comprehensive Hydrogen Bond Theory*, Oxford University Press, 2009.
48 K. G. Chattaraj, R. Paul and S. Paul, *Langmuir*, 2020, **36**(7), 1773–1792.
49 J. H. Jordan and B. C. Gibb, *Chem. Soc. Rev.*, 2015, **44**(2), 547–585.
50 H. F. Ulrich, T. Klein, Z. Zhao, *et al.*, *Small*, 2025, **21**(44), e05481.
51 Y. Mai and A. Eisenberg, *Chem. Soc. Rev.*, 2012, **41**(18), 5969–5985.
52 J. Matern, Y. Dorca, L. Sánchez, *et al.*, *Angew. Chem., Int. Ed.*, 2019, **58**(47), 16730–16740.
53 K. Fischer and M. Schmidt, *Biomaterials*, 2016, **98**, 79–91.
54 M. M. Modena, B. Rühle, T. P. Burg, *et al.*, *Adv. Mater.*, 2019, **31**(32), 1901556.
55 W. Burchard, Solution Properties of Branched Macromolecules, in *Branched Polymers II*, ed. J. Roovers, Springer Berlin Heidelberg, 1999, pp. 113–194.
56 A. Müller and W. Burchard, *Colloid Polym. Sci.*, 1995, **273**(9), 866–875.
57 T. Choisnet, D. Canevet, M. Sallé, *et al.*, *Chem. Commun.*, 2019, **55**(64), 9519–9522.
58 S. Han, E. Nicol, F. Niepceron, *et al.*, *Macromol. Rapid Commun.*, 2019, **40**(3), 1800698.
59 R. Appel, J. Fuchs, S. M. Tyrrell, *et al.*, *Chem. – Eur. J.*, 2015, **21**(52), 19257–19264.